Chemical Engineering & Processing: Process Intensification 205 (2024) 110019

Contents lists available at ScienceDirect

Chemical Engineering and Processing - Process Intensification

journal homepage: www.elsevier.com/locate/cep

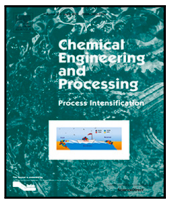

Performance of a RuCs/MgO catalyst coated on additive manufactured support structures via electrophoretic deposition for ammonia synthesis

Linus Biffar [a,*], Anh Thi Pham [a], Walther Benzinger [a], Peter Pfeifer [a,b]

[a] Karlsruhe Institute of Technology, Institute for Micro Process Engineering, Hermann-von-Helmholtz-Platz 1, Eggenstein-Leopoldshafen, 76344, Baden-Württemberg, Germany
[b] INERATEC GmbH, Siemensallee 84, Karlsruhe, 76187, Baden-Württemberg, Germany

ARTICLE INFO

Keywords:
Ruthenium-based catalysts
Additive manufactured fluid guiding elements
Electrophoretic deposition
Ammonia synthesis

ABSTRACT

This work investigates the electrophoretic deposition of a catalytic coating on so-called fluid guiding elements (FGE) with a ruthenium-based catalyst for use in ammonia synthesis reactors. FGE are additive manufactured metallic pipe inserts that have shown to enhance the heat transfer compared to empty pipes by dividing the fluid flow and alternately guiding the partial flows to the wall. Consequently, they could improve the performance of temperature sensitive structured catalytic systems. To be able to demonstrate the degree of process intensification, the required steps to enable the deposition of a reference catalyst for ammonia synthesis are developed. Further, the distribution of catalytically active compounds is characterized. The catalytic activity is assessed in a plug flow reactor under pressures up to 5 MPa and compared against a fixed bed from the same batch. The expected activity from the reference catalyst is calculated by a kinetic rate expression. The coating process does not affect catalytic activity, but a steady deactivation and high sensitivity to feed gas impurities are observed. Possible mechanisms for the deactivation are examined and discussed.

1. Introduction

Green ammonia is a promising candidate for a large scale and carbon-free chemical energy carrier [1]. Its high volumetric energy density in liquid state combined with a high boiling point when compared to other chemical energy carriers such as synthetic natural gas or hydrogen are favorable when it comes to transporting large quantities over long distances [2]. Most state-of-the art ammonia synthesis plants use natural gas as feedstock for the production of hydrogen [3], which enables a stationary operation of the Haber–Bosch loop and the synthesis reactor. For the production of green ammonia however, hydrogen is obtained via electrolysis, which again is powered by renewable energies. Most of these renewable energy sources are volatile in nature, which complicates the stationary operation of the synthesis plant. When designing any power-to-x plant to run in conjunction with fluctuating renewable energies, the load-flexibility of the plant therefore becomes of great importance, since the amount of necessary tanks to buffer these fluctuations can quickly add up [4].

In an ammonia synthesis reactor, the temperature-conversion path of the reaction is a critical design aspect since higher temperatures accelerate the dissociative adsorption of nitrogen on the catalyst, which is the generally accepted rate determining step of the reaction [5], but can also slow down the reaction above a certain temperature once the thermodynamic equilibrium is approached. This leads to the existence of an optimal reaction trajectory for the temperature in dependence of the conversion, which is called the max-rate-curve [6]. Typical industrial ammonia converters are utilizing an adiabatic three-bed design with different configurations of internal or external heat exchangers to optimize the inlet temperature, feed split ratio and catalyst loading of each bed in order to approach the max-rate-curve [7].

As the max-rate-curve is only roughly approximated with this approach, there is an opportunity to reduce the necessary amount of catalyst by designing a reactor which follows the optimal reaction trajectory more closely. This would reduce the size of the reactor and therefore lower its thermal inertia, potentially improving the start-up time and load-flexibility of the plant. One possibility to improve the reaction trajectory is to utilize alternative non-adiabatic reactor technologies like cocurrent-flow or counter-flow designs [6].

Since the reaction is highly exothermic (Eq. (1)), high heat transfer coefficients are necessary to avoid the formation of hotspots in the catalyst bed. This is a challenge in the design of any non-adiabatic reactor, since the heat transfer inversely correlates with the dimension of the pipe or gap which the gas is flowing through. This correlation leads to another challenge, because smaller dimensions generally increase the pressure drop. Since the compression of the recycle gas is a major cost

* Corresponding author.
E-mail address: linus.biffar@kit.edu (L. Biffar).

https://doi.org/10.1016/j.cep.2024.110019
Received 16 April 2024; Received in revised form 4 October 2024; Accepted 5 October 2024
Available online 11 October 2024

factor especially in low pressure ammonia synthesis [8], an increased pressure drop could significantly increase the energy demand of the Haber–Bosch loop.

$$3\,H_2 + N_2 \rightleftharpoons 2\,NH_3 \quad \Delta_R H^0_{298} = -91.4\,\mathrm{kJ\,mol^{-1}} \tag{1}$$

A possible approach to these problems is coating additive manufactured fluid guiding elements (FGE) [9] with catalyst. By applying the catalyst as a coating, the gas flows through the structures unobstructed, which potentially decreases the pressure drop when compared to a fixed bed configuration. In this work, we take the first steps towards this idea and investigate the electrophoretic deposition of a ruthenium-based catalyst [5,10,11] on an additive manufactured metallic support sample. The adhesion and homogeneity of the coating are examined and the catalytic activity of the coating is compared against the reference catalyst and a fixed bed from the same catalyst batch. Furthermore, the long-term deactivation under fluctuating temperature is presented and possible causes for this deactivation are examined and discussed.

Typical examples of conventional catalytic pipe inserts are monoliths or honeycombs, gyroid structures or open-cell foams. They are suited for processes involving high volumetric flow rates due to their low pressure drop and provide a high surface-to-volume ratio enhancing the mass and heat transport [12]. The primary radial heat transfer mechanism in monoliths or honeycomb structures is conduction as fluid channels do not change their position and therefore no heat is transported in the radial direction via convection. Gyroid-like structures can improve the thermal performance of monolithic structures by introducing additional convective heat transfer, which appears to be directly linked to the increased vorticity of the fluid [13]. Current research suggests that the predominant heat transfer mechanism in open-cell foams is conduction via the continuous solid phase [14,15]. Our patented fluid guiding elements work on a different principle as the fluid flow is divided into multiple partial flows [9]. At defined distances, the position of two adjacent partial flows is swapped alternately. With this approach, each partial flow is guided from the center of the pipe to the wall and back without getting into contact with fluid from the other channels and heat is transported in radial direction via convection, which greatly increases the integral heat transfer coefficient [16].

To demonstrate the improved heat and mass transfer due to these fluid guiding elements under reactive conditions, we chose the process of ammonia synthesis. In this paper we address the coating procedure with a reference catalyst selected from literature. It is of utmost importance for the demonstration of process intensification that the coating is homogeneous and comparatively thick so that the amount of catalyst in the system is maximized without loosing efficiency through internal mass transport limitation and that homogeneous contact with the gas phase is ensured.

Several options exist to deposit an impregnated catalyst on a substrate as a coating, including washcoating, sol–gel deposition and electrophoretic deposition. To enable a deposition of powder from a suspension via the washcoating process, a binder and a pH-altering additive is usually necessary [17], which is not ideal for the deposition of an impregnated catalyst since the active compounds or promoters can be dissolved and lost in the process. When following the sol–gel method or electrophoretic deposition, typically only a thin coating ranging between <1 - 50 µm is applied [17], which is sufficient when the effective reaction rate is mostly limited by diffusion. For reactions controlled by the intrinsic reaction rate like ammonia synthesis however, the effective reaction rate is directly linked to the catalyst loading and thick coatings are advantageous. With coating techniques involving a deposition from a particle suspension, this leads to problems as internal tensions develop during the drying process which can lead to cracks and subsequent flaking of the coating [18,19]. With the successive deposition of multiple thin layers it is possible to circumvent this limitation, but this process can become time-consuming when using the sol–gel method since the gelation of each layer needs to be completed before applying the next layer [20]. The coating process can therefore be greatly accelerated by utilizing electrophoretic deposition, since the next layer can be applied directly after the solvent is evaporated from the wet coating. Multilayer deposition has been successfully used in ceramic applications to apply dense zirconia coatings [21] or more porous Al_2O_3/Y−TZP coatings with the addition of a binder [22]. In this work, we investigate the performance of a porous and thick catalytic coating applied via multilayer electrophoretic deposition without the use of a binding agent on fluid guiding elements, which improve the heat transfer by controlled redirection of flow and do not require the contribution of solid heat transport.

2. Methods

2.1. Additive manufactured support structures

Fluid guiding elements were designed in `Autodesk Inventor` and manufactured via selective laser melting (Realizer SLM 125). The wall thickness of the FGEs was 180 µm and the total length 50 mm. The stainless steel powder (316 L) was melted with a laser spot size of 25 µm and a powder layer height of 30 µm. Before applying the coating, the FGEs were cleansed in an ultrasonic bath.

2.2. Catalyst preparation

The catalyst preparation was adapted from [10] and utilizes a two-step wet impregnation method, subsequently adding both active compounds ruthenium and cesium to the magnesium oxide support. To begin, the magnesium oxide (MgO, Sintermagnesia, 200 Mesh, Magnesia GmbH) was crushed down via wet milling with ethanol (EtOH, >99.9% purity, VWR) in a ball mill (Retsch PM 100 CM) to a Sauter-diameter of about 2.5 µm. The suspension was diluted with ethanol until a loading of 50 mg mL^{-1} was reached. The necessary amount of the precursors ruthenium-acetylacetonate (Ru−acac, >97% purity, Sigma-Aldrich) and cesium carbonate (Cs_2CO_3, >99% purity, Sigma-Aldrich) was determined so that the desired mass fraction of ruthenium w_{Ru} and the molar ratio of cesium per ruthenium v are met in the final catalyst:

$$m_{\mathrm{Ru-acac}} = \frac{m_{\mathrm{MgO}} w_{\mathrm{Ru}} M_{\mathrm{Ru-acac}}}{M_{\mathrm{Ru}}\left(1 - w_{\mathrm{Ru}}\right) - v w_{\mathrm{Ru}} M_{\mathrm{Cs}}}$$

$$m_{\mathrm{Cs_2CO_3}} = \frac{m_{\mathrm{MgO}} v w_{\mathrm{Ru}} M_{\mathrm{Cs_2CO_3}}}{2\left(M_{\mathrm{Ru}}\left(1 - w_{\mathrm{Ru}}\right) - v w_{\mathrm{Ru}} M_{\mathrm{Cs}}\right)}$$

The first precursor Ru−acac was dissolved in the suspension and stirred for 4 h under atmospheric conditions. The solvent was then evaporated in a rotary evaporator at a temperature of 60 °C and a pressure of 200 mbar. To decompose the precursor, the dark-red powder was placed in a muffle furnace at 170 °C for 5 h under ambient atmosphere. The resulting agglomerates were crushed in a ball mill. After the second precursor Cs_2CO_3 was solved in ethanol, the Ru−MgO powder was added, and the suspension was stirred for 4 h under atmospheric conditions. The ethanol was again removed in a rotary evaporator.

2.3. Electrophoretic deposition

After adding cesium to the catalyst powder via the precursor Cs_2CO_3, the zeta potential of the particles in the suspension dropped (see Section 3.1), making the suspension susceptible to the formation of agglomerates. These agglomerates were found to prevent the formation of a thick adhesive coating and a dispersant additive (ZetaSperse 1200, Evonik) was added to sterically hinder the formation of agglomerates as demonstrated in Fig. 1. Steric stabilization occurs when the long molecules of the dispersant additive attach on the colloidal particles, physically preventing them from getting close enough to each other that agglomerations could form [23].

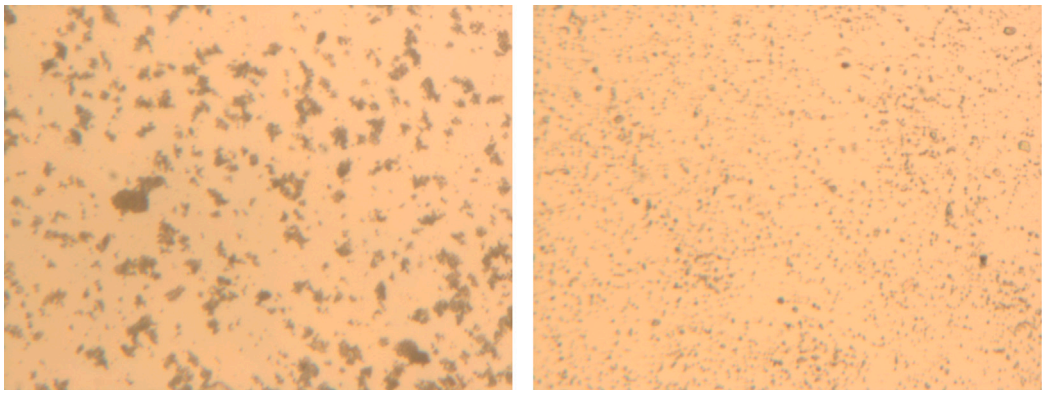

(a) No additives. (b) 20 wt.% ZetaSperse 1200.

Fig. 1. Agglomeration of catalyst particles in suspension, $10\,mg\,mL^{-1}$ RuCs/MgO in Ethanol. Optical microscope, 225x magnification.

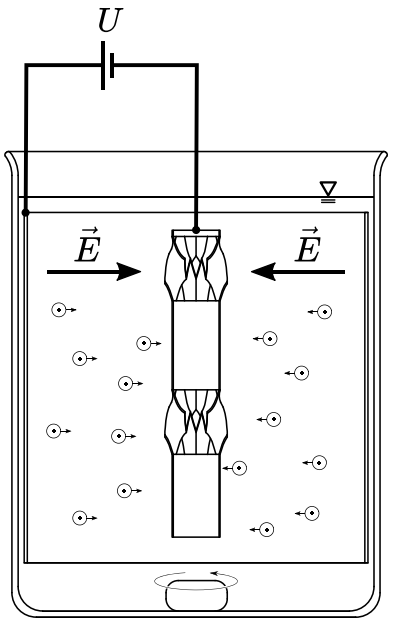

(a) Setup for electrophoretic deposition.

(b) Various FGE samples. A: Uncoated metallic support. B: Fresh coating, 209.8 mg catalyst. C: Coating after 500 h in reactor, 201.7 mg catalyst.

Fig. 2. Electrophoretic deposition of catalyst.

For the electrophoretic deposition, the suspension was slowly stirred in a 80 mL beaker to prevent a sedimentation of particles. A thin sheet metal was placed inside the beaker as a counter-electrode and connected with the power supply. The metallic support was then submerged in the suspension and connected to the power supply as well. A voltage of 50 V was applied for 1 - 3 min, depending on the solid loading of the suspension [24]. To achieve crack-free coatings with a thickness of 100 µm or more, it was necessary to deposit the desired catalyst mass in multiple successive layers of about 20 µm per layer. After each layer, the coating was dried at room temperature before depositing the next layer. This way, the buildup of internal tensions during the drying process was minimized [18], and a homogeneous and crack free coating could be achieved. The experimental setup and coated samples are shown in Fig. 2.

2.4. Activity measurements

Hydrogen and nitrogen (Alphagaz 2, 6.0 Purity, Air Liquide) were dosed via calibrated mass flow meters (Brooks SLA 5850). Upstream of the reactor, a molecular sieve (Molesieve 3 A, Sigma-Aldrich) was installed to remove moisture which might enter the system while changing the catalyst or the gas bottles. The molecular sieve was activated at 200 °C in a vacuum oven. The reactor consists of three independently heated brass heating jackets with a length of 95 mm each, wrapping a stainless steel tube with a diameter of 0.5 inch to ensure an isothermal zone around the central heating jacket. The coated catalyst sample was placed on top of uncoated FGE and aligned with the middle heating jacket. The temperature in the center of the reactor was recorded with a thermocouple inside a 0.125 inch tube. After cooling the gas to ambient temperature, a back pressure regulator (Equilibar LF Research Series) was used to control the system pressure.

The product gas was analyzed using a gas chromatograph (GC, Agilent HP 6890, modified by Teckso). A stop-flow valve ensured a constant pressure in the sample loop before admitting the sample to the column (CP-Volamin, CP7448, 60 m × 0.32 mm). A thermal conductivity detector was then used to record the chromatogram. The ammonia peak was calibrated with a reference gas mixture (basi Schöberl) and the water peak by saturating the gas stream with moisture by bubbling through a washing flask with known temperature and pressure.

Before each experiment, the lines were flushed using a bypass, then the catalyst sample was dried inside the reactor at 115 °C in

Table 1
Parameters used for kinetic rate expression [10].

w_{Ru}	2	wt.%
$n_{H\ per\ Ru}$	0.95	–
$k_{1,0,f}$	56	kPa s^{-1}
$k_{1,0,b}$	2×10^{10}	s^{-1}
$\Delta_{ads}H_{N_2}$	−105.0	kJ mol^{-1}
$K_{2,0}$	1.81×10^{-4}	atm^{-1}
$\Delta_{ads}H_{H_2}$	−81.8	kJ mol^{-1}
$E_{A,1}$	32.5	kJ mol^{-1}

flowing nitrogen for 8 h. The reduction of the catalyst was carried out in synthesis gas with a temperature ramp of 20 K h^{-1} to a maximum temperature of 450 °C. Each parameter variation was held until a steady state at the GC was reached, which typically took between 1 - 2 h.

For the experiments, a FGE was coated with 201.7 mg of catalyst powder as described in Section 2.3. From the same catalyst batch, a fixed bed was prepared to compare the activity of the coating. This was done by pressing the prepared catalyst powder to pellets, subsequently crushing and sieving them to a range of 150 - 300 µm. The fixed bed was diluted with silicon carbide to reduce possible axial diffusion effects. The total catalyst mass used for the fixed bed was 202.6 mg.

2.5. Kinetic comparison

In order to enable the electrophoretic deposition of the catalyst, different solvents and precursors were used and a dispersing agent was added. As this could affect the catalytic activity, a reference kinetic was implemented as proposed by McClaine et al. [10] to benchmark the activity of the catalyst. The implementation was validated using data from the original publication. The kinetic expression is a LHHW-type equation:

$$\frac{d\dot{n}_i}{dm_{cat}} = \nu_i \frac{k_1 n_{ads} p_{N_2} \left(1 - \frac{p_{NH_3}^2}{p_{H_2}^2 p_{N_2}} \frac{1}{K_p^2}\right)}{\left(1 + \sqrt{K_2 p_{H_2}} + \frac{\sqrt{K_1}}{K_p} \frac{p_{NH_3}}{p_{H_2}^{3/2}}\right)^2} \tag{2}$$

The equilibrium constant $K_P(T)$ was determined by minimizing the free Gibbs enthalpy for a given temperature, pressure and gas composition [25]. Ideal gas behavior was assumed when calculating the fugacity of the compounds, which might lead to inconsistencies regarding the equilibrium composition especially at higher pressures. To find the minimum of the constrained and nonlinear objective function, the MATLAB function `fmincon` was used. The parameters for the rate expression are given in Table 1. The Bodenstein number was checked to ensure a plug-flow-reactor (PFR) behavior could be assumed. The gas composition at the exit of the reactor was then calculated by numerically integrating the kinetic rate expression (Eq. (2)) with the MATLAB integration routine for ordinary differential equations `ode45`.

2.6. Electron probe microanalysis

A field emission electron probe microanalyzer (Jeol JXA-8530F) was used to analyze the distribution of the active elements cesium and ruthenium. To investigate the cross-section of the coating, the coated sample was embedded in epoxy resin, cut and a conductive carbon layer was applied. The distribution of both active metals was analyzed via wavelength dispersive X-ray spectroscopy (WDX) maps with an accelerating voltage of 15 kV and a current of 20 nA. The surfaces of both coated and uncoated FGE were analyzed via energy-dispersive X-ray spectroscopy (EDX).

2.7. Scanning transmission electron microscopy

The sample was prepared at room temperature in air by drop-casting of a diluted suspension of nanoparticles dispersed in ethanol onto a commercial holey ultrathin amorphous carbon film (3 nm) mounted on 400 µm mesh Cu grid (Plano 01824). The size, shape and the chemical composition of Ru – Cs nanoparticles on the MgO substrate was investigated by high-angle annular dark-field (HAADF) scanning transmission electron microscopy (STEM) in combination with EDX carried out on an FEI Osiris ChemiSTEM microscope at 200 keV electron energy, which is equipped with a Super-X EDX system comprising four silicon drift detectors (Bruker).

3. Results and discussion

3.1. Catalyst preparation and electrophoretic deposition

Since Ru – acac was used in the preparation of the catalyst instead of $Ru_3(CO)_{12}$ as proposed by McClaine et al. [10], the preparation had to be adjusted as the original decomposition temperature lead to the formation of a ruthenium mirror on the crucible, which suggests an evaporation and subsequent precipitation of the precursor Ru – acac similar to the observations by Aika et al. [26]. A thermogravimetric analysis was performed in synthetic air on Ru – acac Appendix A. The decrease in weight begins at 170 °C, consequently this temperature was chosen for the decomposition. During the decomposition process the powder changed from orange-gray to an ashen color, indicating a successful decomposition of the acetylacetonate. No formation of ruthenium depositions on the crucible were observed at this decomposition temperature.

Preliminary experiments showed that the coating of the catalyst support structures was working as expected when using sintered and milled MgO powder. After impregnation with both active metals however, agglomerates were found in the suspension (Fig. 1), which prevented a deposition of particles on the substrate. This was likely caused by a drop of the zeta-potential of the particles in the suspension from 41.4 mV with MgO in EtOH to 10.7 mV with MgO – Ru – Cs_2CO_3 in EtOH. This drop can be attributed to an increased number of free ions in the suspension from the second precursor Cs_2CO_3 [19,27]. It has been shown that the organic dispersion agent was decomposed during the reduction of the catalyst as it had no influence on the catalytic activity (see Section 3.2).

To deposit a catalyst mass of about 200 mg, a multilayer deposition was used to avoid the formation of cracks during the drying process (Section 2.3). Utilizing this approach it was possible to deposit layers up to a thickness of about 300 µm. Depositing thicker layers lead to the formation of cracks and the adhesion of the coating was greatly reduced as shown in the supplementary material. Cross-section WDX maps of a sample coated with 194.0 mg catalyst are presented in Fig. 3. The layer thickness of the catalytic coating is about 135 µm. For ruthenium, no gradients in the intensity of the signal are noticeable over the layer thickness. Multiple small peaks indicate the presence of catalyst particles with a higher concentration of ruthenium, possibly because the precursor Ru – acac was not yet fully dissolved in the suspension before starting the drying process. Since these particles appear to be randomly distributed, this higher ruthenium concentration seems to have no effect on the deposition process. For cesium, a few spots with higher concentration near the coating–substrate interface and a slight gradient near the surface of the coating are observed. Since the distribution of the promoter is still mostly uniform, the effect on the overall catalytic activity should be negligible. The images also show a high porosity of the coating, reducing the risk of possible diffusion limitations which could arise from concentration gradients over the layer thickness. Utilizing a dispersing agent and a multilayer deposition, a homogeneous and porous coating has been achieved.

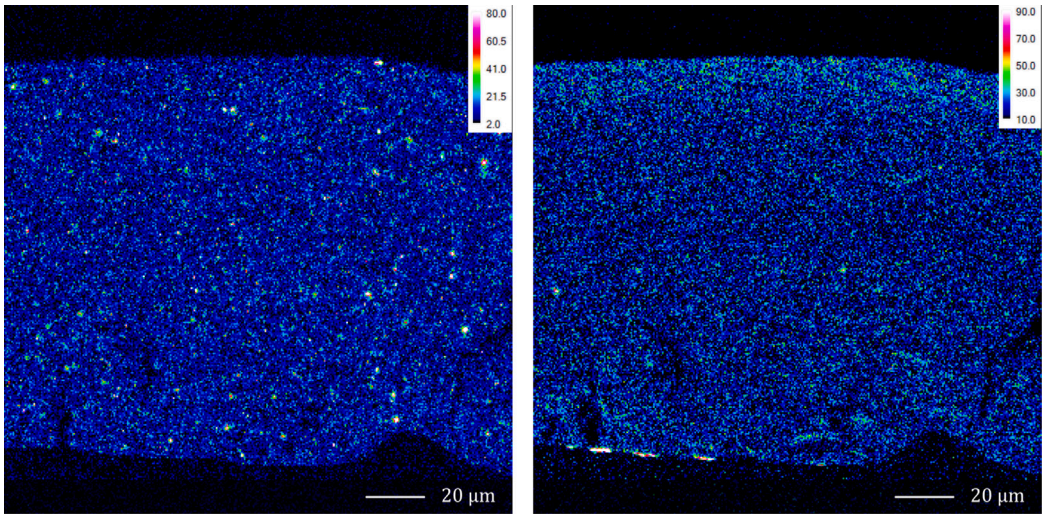

(a) Ruthenium (L-α) (b) Cesium (L-α)

Fig. 3. WDX maps: Element distribution of catalytic active compounds in coating cross-section.

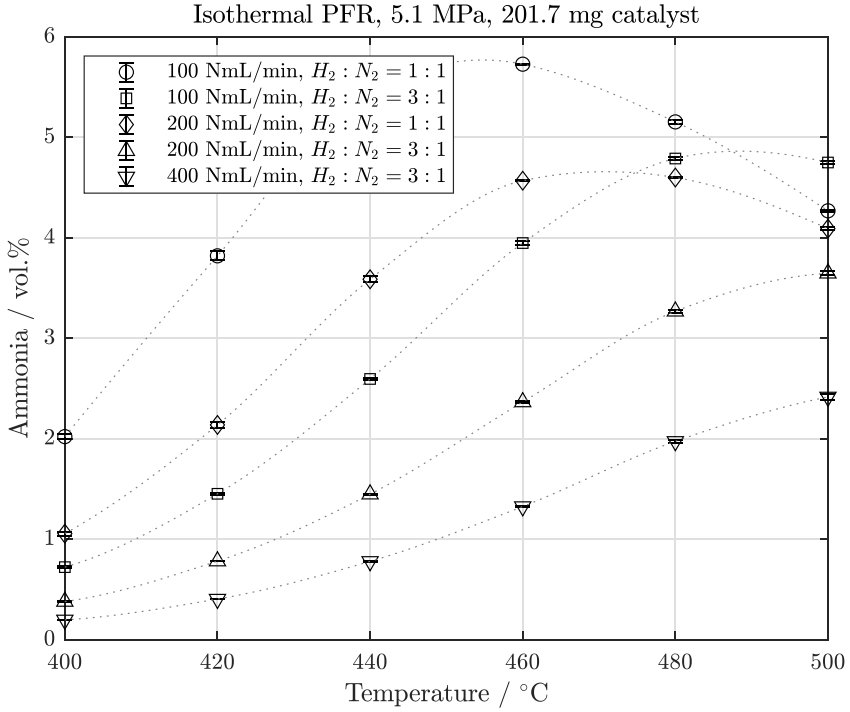

Fig. 4. Activity measurements of coated sample. Dotted lines for visualization purposes only.

3.2. Catalytic activity

Five different gas feeds were measured at different temperatures ranging from 400 - 500 °C at a pressure of 5 MPa for a total number of 30 data points (Fig. 4). For the gas feeds with a non-stoichiometric ratio of hydrogen and nitrogen of $\frac{H_2}{N_2} = 1$, higher ammonia concentrations are observed, which is caused by the competitive adsorption of hydrogen on the catalyst surface limiting the reaction rate when running the reaction at higher stoichiometric ratios [5,6,28]. At higher temperatures, the conversion becomes more and more limited by the thermodynamic equilibrium of the exothermic reaction (Eq. (1)).

To examine if the electrophoretic deposition of the catalyst powder affected the activity of the catalyst especially considering the added dispersing agent or if the coating introduced mass transport limitations, an identical experiment was conducted with a fixed bed from the same catalyst batch. In Fig. 5(a), the ammonia concentration in the product stream of the catalytic coating is scattered against the concentration of the corresponding data point from the fixed bed experiment. At higher ammonia concentrations, a low deviation between the experiments is observed, which is expected as the thermodynamic equilibrium composition is approached. Since both experiments are in good agreement at lower temperatures as well, the coating procedure did not affect the catalytic performance and the porosity of the deposited layer is sufficient to prevent diffusion limitations.

When comparing the data points against the expected ammonia concentration as calculated by the reference kinetic in Fig. 5(b) (see Section 2.5), a higher activity than expected was reached at lower ammonia concentrations. As the thermodynamic equilibrium is approached, a lower concentration is observed. A possible explanation

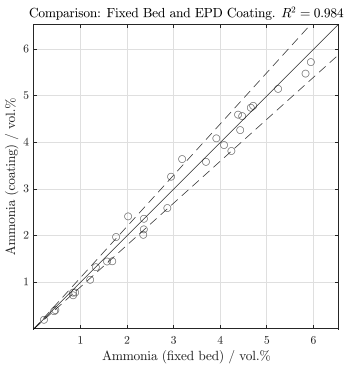

(a) Comparison with fixed bed from same catalyst batch.

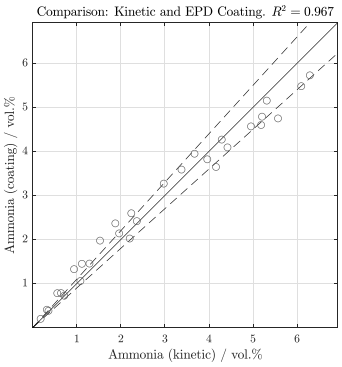

(b) Comparison with reference kinetic [10].

Fig. 5. Benchmarking the catalytic activity of the electrophoretic coating. Parity lines at ±10%.

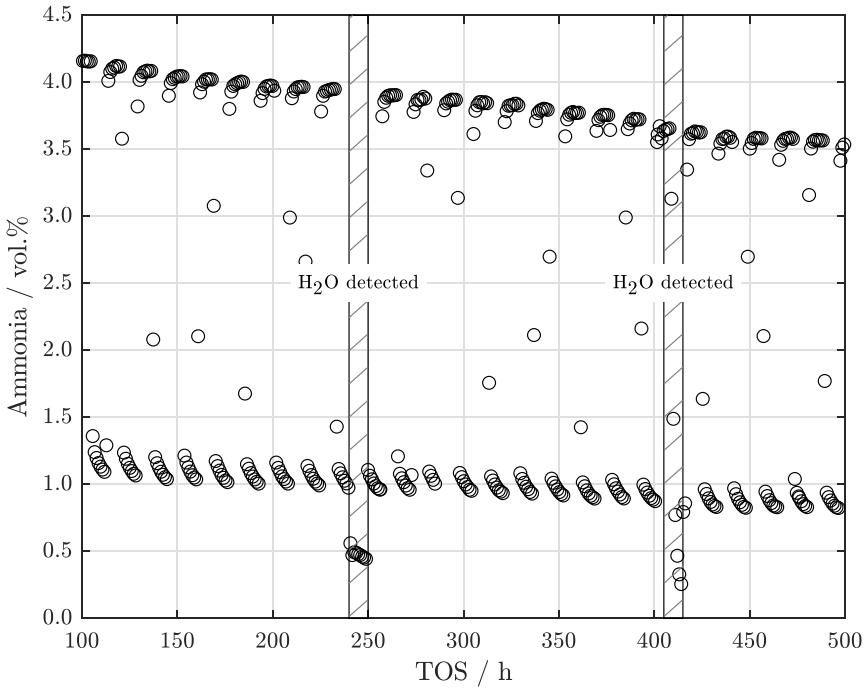

Fig. 6. Long-term deactivation while alternating the temperature between 450 °C and 400 °C.

is that for both the partial pressures in the kinetic expression and the calculation of the equilibrium constant, ideal gas behavior was assumed. As the experiment was conducted at 5 MPa, that assumption might lead to imprecise calculation of these values. As McClaine et al. did not disclose their method to determine the equilibrium constant K_P, the use of a different thermodynamic model or empiric correlation could also explain the deviation. The results of the benchmark are still satisfying considering that the original kinetic was fitted to a dataset recorded at 20.7 atm, a different catalyst preparation was developed, and a consecutive coating procedure was applied.

3.3. Long term stability and catalyst deactivation

To examine the long term stability and activity of the catalyst under fluctuating temperatures, similar to as they could occur during non-stationary operation of an ammonia synthesis reactor, a flow of $100\,\mathrm{N\,mL\,min^{-1}}$ with a stoichiometric ratio of $\frac{H_2}{N_2} = 1$ was dosed while the temperature was changed from 400 °C to 450 °C every eight hours while the pressure was held at 5 MPa (Fig. 6). During the measurements, the measured ammonia concentration dropped significantly for two time periods. After investigating the respective chromatograms, an additional peak was found which was identified to be corresponding to water. As the gas bottles were not changed during the experiment, no other experiment was connected to the lines and a molecular sieve was installed upstream of the reactor, it is unlikely that water entered the system upstream of the reactor. We suspect that a small amount of moisture entered the GC via the carrier gas and absorbed ammonia before being analyzed in the GC, therefore reducing the amount of measured ammonia. After a few hours, the water peak disappeared and the measured concentration continued to follow the general trend again, which is a further indication that water entered the system downstream of the reactor, since the catalyst should have been notably less active afterwards otherwise.

A continuous loss of activity is observed, which according to literature can be attributed to several mechanisms. To investigate if cesium was leaching as proposed by [29], we removed the metallic support structure downstream of the coated sample and analyzed the composition of its surface via EDX. Small clusters were found on the structure which contained cesium (Fig. 7), which is not present in the areas around these clusters. Since the promoter layer on the catalyst

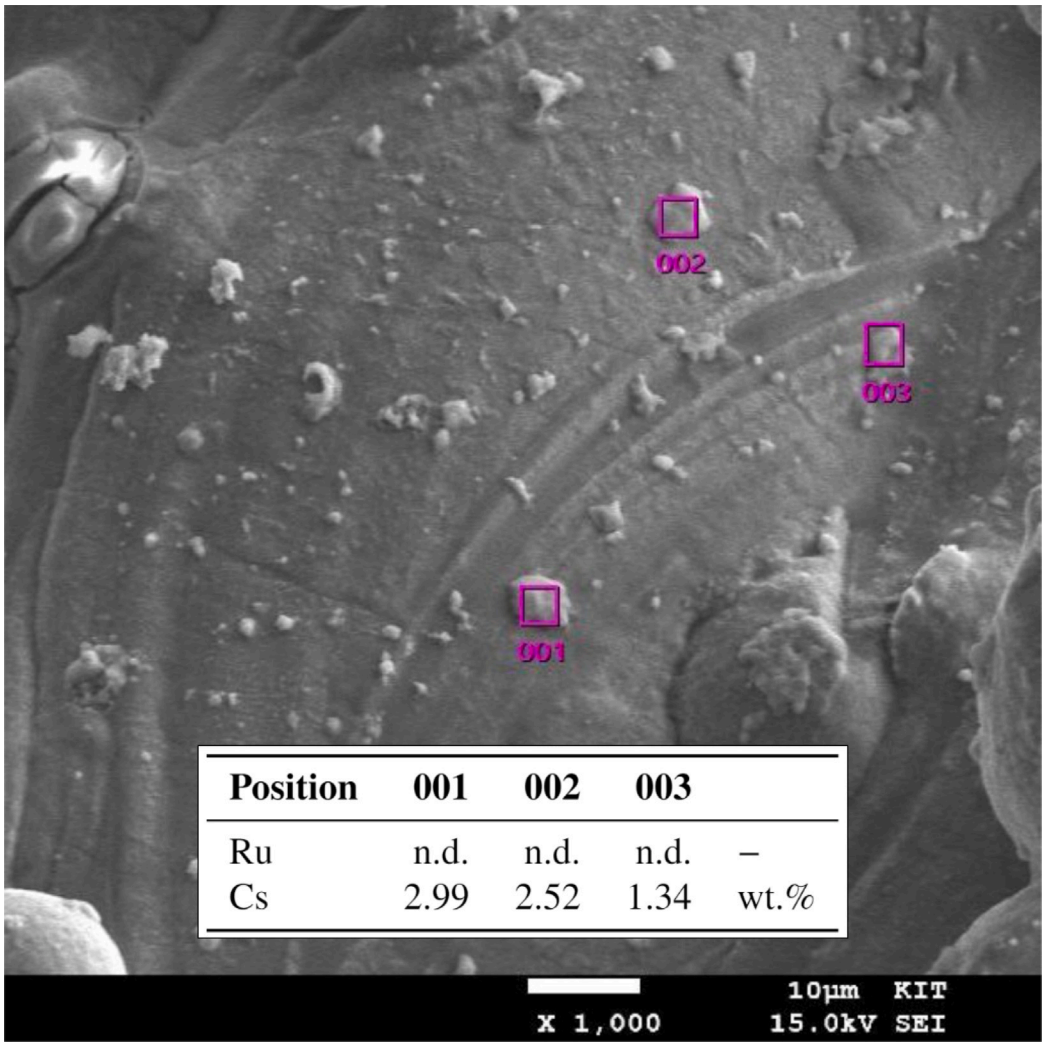

Fig. 7. Cesium clusters found on uncoated support structures placed downstream of catalyst sample. Weight percent determined via EDX.

is thought to mainly consist in the form of $Cs_{2+x}O$ after the initial reduction step [30], it can react to Cs_2O and Cs_2O_2 in the presence of even minuscule amounts of oxygen. These cesium compounds have a low melting point of 297.8 °C and 490 °C respectively [29]. Further it was found that cesium species have a low affinity to basic supports such as MgO [28]. These findings support the leaching of Cs as a plausible deactivation mechanism. No ruthenium was detected on the support structure. To further test this hypothesis, a similar catalyst was synthesized replacing cesium with barium as suggested by Bielewa et al. [31]. As shown in the supplementary material, we did not see any substantial deactivation of the barium-promoted catalyst in a long-term experiment conducted over 1000 h, which supports the assumption that the leaching of cesium is a major factor in the deactivation of the RuCs/MgO catalyst.

Another mechanism to discuss is the surface diffusion and agglomeration of ruthenium atoms resulting in a loss of dispersion and therefore active catalyst sites [32–34]. After the long-term experiment, catalyst was scraped off, examined via STEM-EDX images and compared to fresh catalyst from the same batch. For both examples, three particles were analyzed (Fig. 8). While we did find one particle with a high dispersion of ruthenium in the fresh batch (Fig. 8(a), second image) similar to the findings of [29], the other two particles showed the presence of larger ruthenium clusters even before the sample was placed in the reactor. Fig. 8(b) shows three different particles which were analyzed after 500 h in synthesis conditions (see Fig. 6). While two of these images show larger clusters, the top image shows the presence of smaller cluster as well. With only these few images, no clear conclusion about the magnitude of the effect of ruthenium or cesium surface diffusion in this experiment can be drawn.

The sintering of micropores is discussed as another possible deactivation mechanism [29]. Analysis via nitrogen physisorption showed that no micropores were present in the fresh catalyst powder (see Appendix B), which is expected since sintered magnesium oxide was used as a support material, which should not have a porous structure. The loss of internal surface area can therefore be discarded as a possible explanation for the long-term deactivation of this catalyst.

From Fig. 6 it can be concluded that some time is needed when switching back and forth between 400 °C and 450 °C. This is mostly due to the thermal inertia of the reactor itself and not related to the kinetics of the reaction.

This steady deactivation poses a major challenge to any potential industrial application of this catalyst whether it is used in pressed form or as a coating, since established wustite-based catalysts can exceed lifetimes of 10 years [35].

4. Conclusion and outlook

A RuCs/MgO catalyst was synthesized with an adapted recipe taking the subsequent coating procedure into consideration. In order to enable the electrophoretic deposition of the catalyst powder, a dispersant

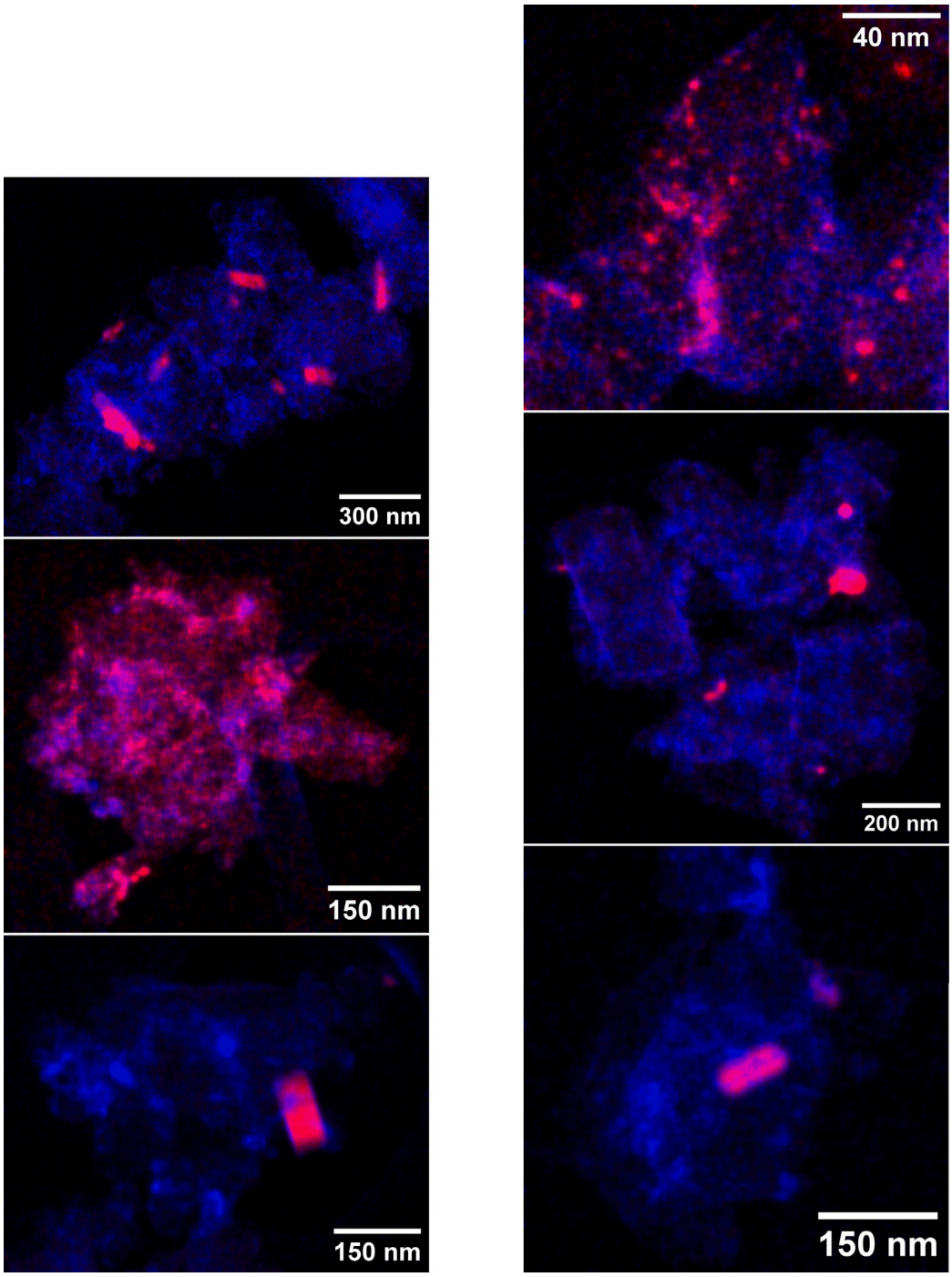

(a) Fresh catalyst.

(b) Catalyst after 500 h in reactor.

Fig. 8. STEM-EDX maps of Ru-Cs distribution. Red: Ruthenium (Ru$-L_{\alpha}$), Blue: Cesium (Cs$-L_{\alpha}$).

additive was added to the suspension to sterically hinder the formation of agglomerates. Homogeneity in overall catalyst and active species distribution are, alongside with high resistivity of the coating to thermal gradients regarding adhesion, of utmost importance for process intensification. Utilizing a multilayer deposition approach, a porous and homogeneous coating layer could be deposited on the additive manufactured metallic support structures. No radial gradients or cracks were found when examining the cross-section of the catalytic coating. In experimental measurements taken in a lab-scale PFR reactor, the catalytic activity of the coating matched the activity of the catalyst powder and was in good agreement with kinetic calculations from a reference catalyst used as a benchmark. However, even with a gas purity of 6.0 in combination with a molecular sieve, a steady deactivation was observed, likely attributed to either the leaching of cesium or the surface diffusion and agglomeration of ruthenium or cesium. This poses a challenge for potential industrial applications of this catalyst regardless if it is used in form of pressed pellets or as a coating.

In future works, it should be investigated if the same coating procedure can be applied to industrially established wustite-based catalysts, as the two major benefits of utilizing coated fluid guiding elements (low pressure drop and high integral heat transfer coefficients) are not directly dependent on the choice of catalyst. Since the coating process

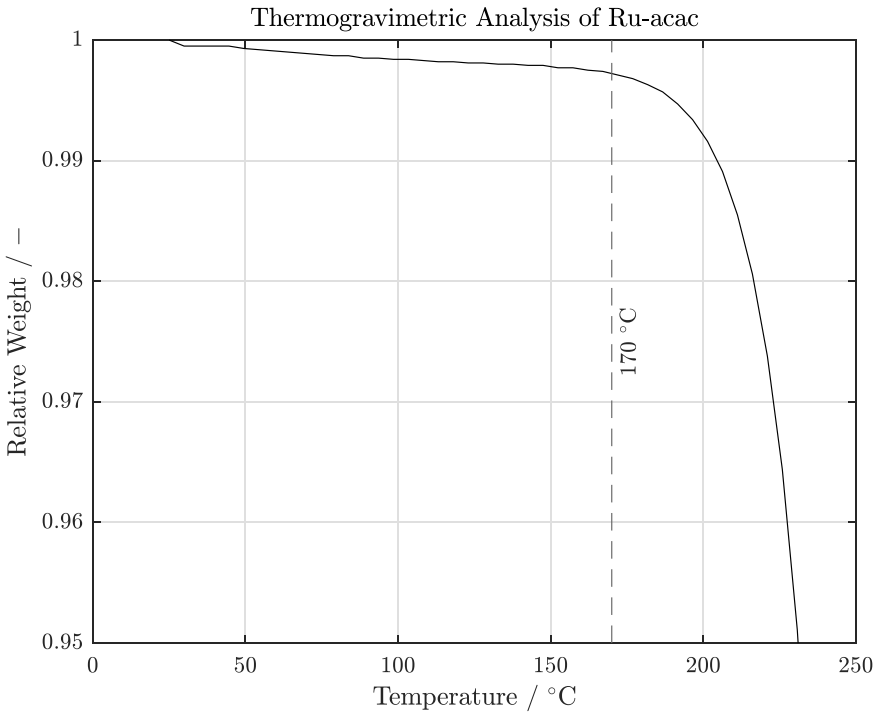

Fig. A.9. TGA of Ru–acac.

is time-consuming at the moment due to the repeated drying steps between each deposited layer, an effort must be made to automate the coating process if the technique is to emerge out of lab-scale applications.

CRediT authorship contribution statement

Linus Biffar: Writing – original draft, Visualization, Software, Methodology, Investigation, Formal analysis, Data curation, Conceptualization. **Anh Thi Pham:** Writing – review & editing, Investigation, Data curation. **Walther Benzinger:** Writing – review & editing, Project administration, Funding acquisition, Conceptualization. **Peter Pfeifer:** Writing – review & editing, Supervision.

Declaration of competing interest

The authors declare the following financial interests/personal relationships which may be considered as potential competing interests: Linus Biffar reports financial support was provided by Federal Ministry of Education and Research Berlin Office. If there are other authors, they declare that they have no known competing financial interests or personal relationships that could have appeared to influence the work reported in this paper.

Acknowledgments

The authors would like to thank Luca Eichhorn as a student assistant for his contribution to the sample preparation method, Uta Gerhards and Florian Messerschmidt (both KIT, IMVT) for the WDX analysis, Malina Burcea (KIT, CVT) for the BET measurements, Diana Deutsch (KIT, IKFT) for the TGA analysis and Dr. Radian Popescu (KIT, LEM) for the HAADF-STEM images and EDX maps. Funding has been received from the German Federal Ministry of Education and Research under the project Campfire (03WIR2307B) and is gracefully acknowledged.

Appendix A. Thermogravimetric analysis

A thermogravimetric analysis (TGA) was performed on the precursor Ru–acac to determine an appropriate temperature for the decomposition of acetylacetonate (Fig. A.9). The heating ramp was 10 K min^{-1} and the atmosphere synthetic air. Since Ru–acac has a melting point of 260 °C, high temperatures during the decomposition can lead to a leaching of ruthenium. The decomposition of the precursor started at around 170 °C, after that a fast reduction in weight is observed. Preliminary experiments showed that temperatures higher than 170 °C in the muffle oven lead to the formation of a ruthenium mirror on the crucible when decomposing the impregnated Ru–acac–MgO.

Appendix B. Surface analysis via nitrogen physisorption

The BET surface area was determined to be 18.1 $m^2\,g^{-1}$. In Fig. B.10, a sorption isotherm of type 2 or 3 with a slight hysteresis of type H3 are recognizable, indicating a non-porous solid with weak interactions between the adsorbed molecules and aggregations of plate-like particles [36]. This observation is in agreement with images of a cross-section of the coating taken by electron microscopy, where plate-like particles are present (Fig. B.11). No micropores were therefore present in the studied catalyst.

Symbols

E	J mol^{-1}	activation energy
k	Pa s^{-1}, s^{-1}	rate constant
K	Pa^{-1}	equilibrium constant
n_{ads}	mol kg^{-1}	active sites
$\dot{n}$	mol s^{-1}	molar flow
m	kg	mass
M	kg mol^{-1}	molar mass
p	Pa	pressure
υ	–	stoichiometric ratio
w	kg kg^{-1}	weight fraction
ν	–	stoichiometric coefficient

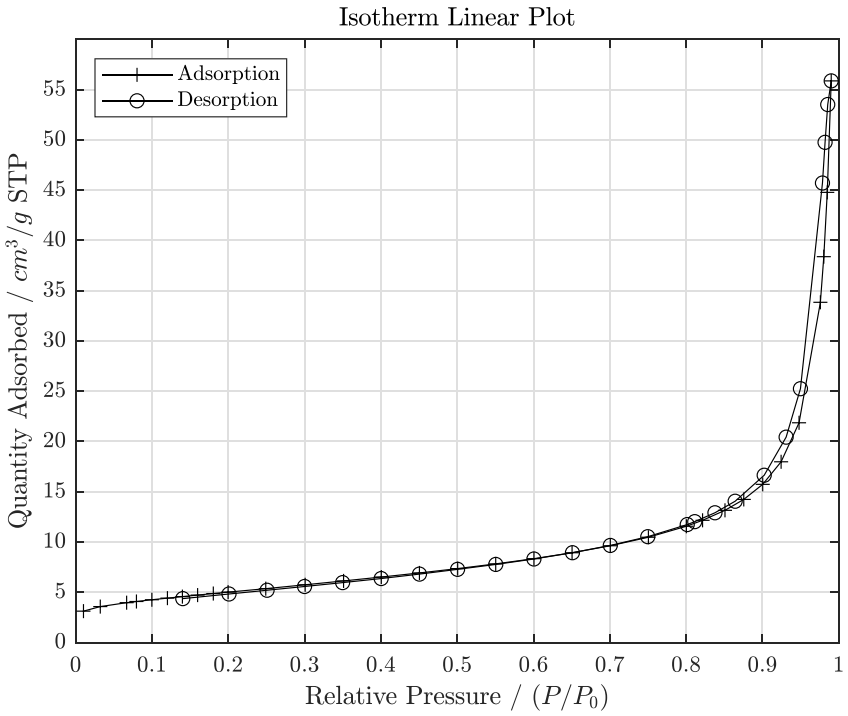

Fig. B.10. BET analysis of RuCs/MgO.

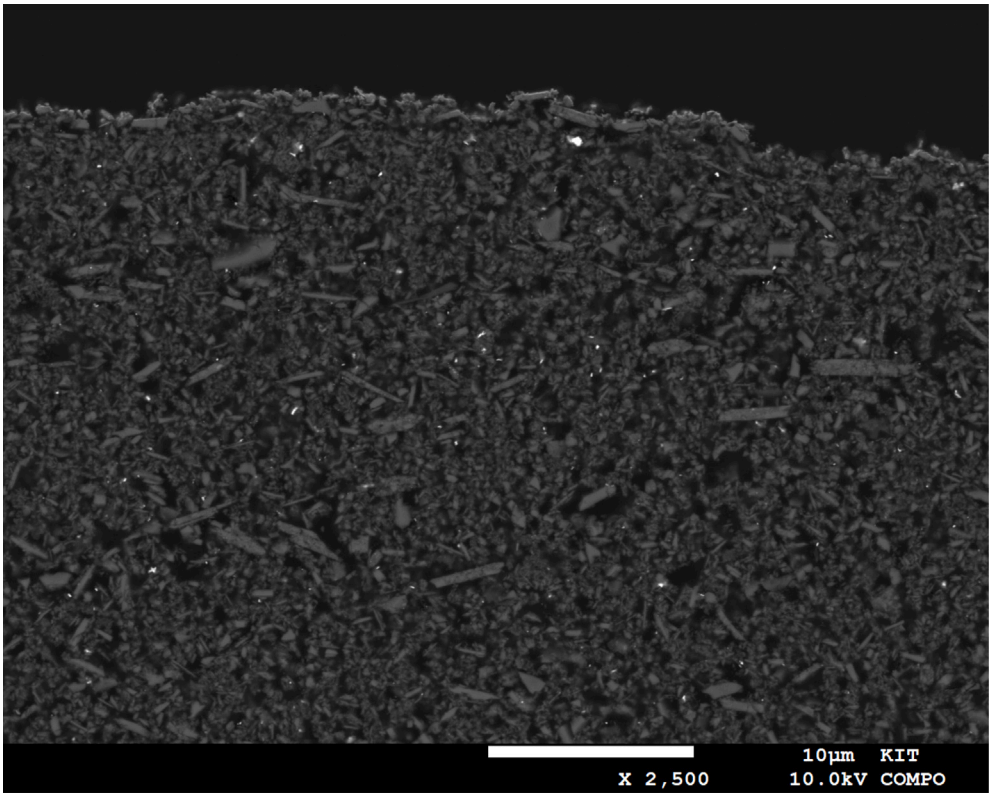

Fig. B.11. Cross-section of coating.

Appendix C. Supplementary data

Supplementary material related to this article can be found online at https://doi.org/10.1016/j.cep.2024.110019.

Data availability

Data will be made available on request.

References

[1] A. Valera-Medina, H. Xiao, M. Owen-Jones, W. David, P.J. Bowen, Ammonia for power, Prog. Energy Combust. Sci. 69 (2018) 63–102, http://dx.doi.org/10.1016/j.pecs.2018.07.001.

[2] J. Guo, P. Chen, Catalyst: NH3 as an energy carrier, Chem 3 (5) (2017) 709–712, http://dx.doi.org/10.1016/j.chempr.2017.10.004.

[3] R. Lan, J.T. Irvine, S. Tao, Ammonia and related chemicals as potential indirect hydrogen storage materials, Int. J. Hydrog. Energy 37 (2) (2012) 1482–1494, http://dx.doi.org/10.1016/j.ijhydene.2011.10.004.

[4] P. Pfeifer, L. Biffar, F. Timm, T. Böltken, Influence of power-to-fuel plant flexibility towards power and plant utilization and intermediate hydrogen buffer size, Chem. Ing. Tech. 92 (12) (2020) 1976–1982, http://dx.doi.org/10.1002/cite.202000084.

[5] O. Hinrichsen, F. Rosowski, M. Muhler, G. Ertl, The microkinetics of ammonia synthesis catalyzed by cesium-promoted supported ruthenium, Chem. Eng. Sci. 51 (10) (1996) 1683–1690, http://dx.doi.org/10.1016/0009-2509(96)00027-9.

[6] M. Appl, Ammonia: Principles and Industrial Practice, Wiley-VCH, Weinheim; New York, 1999, http://dx.doi.org/10.1002/9783527613885.

[7] A. Jess, Chemical Technology: From Principles to Products, second ed., Wiley-VCH Verlag, Weinheim, 2020.

[8] B. Lin, T. Wiesner, M. Malmali, Performance of a small-scale Haber process: A techno-economic analysis, ACS Sustain. Chem. Eng. 8 (41) (2020) 15517–15531, http://dx.doi.org/10.1021/acssuschemeng.0c04313.

[9] E. Hansjosten, A. Wenka, A. Hensel, W. Benzinger, M. Klumpp, R. Dittmeyer, Custom-designed 3D-printed metallic fluid guiding elements for enhanced heat transfer at low pressure drop, Chem. Eng. Process. Process Intensif. 130 (2018) 119–126, http://dx.doi.org/10.1016/j.cep.2018.05.022.

[10] B.C. McClaine, T. Becue, C. Lock, R.J. Davis, Kinetic analysis of ammonia synthesis catalyzed by barium-promoted ruthenium supported on zeolite X, J. Mol. Catal. A Chemical 163 (1–2) (2000) 105–116, http://dx.doi.org/10.1016/S1381-1169(00)00403-9.

[11] H. Hinrichs, J. Niedetzky, Ein Neuer konverter-typ für die ammoniak-synthese, Chem. Ing. Tech. 34 (2) (1962) 88–91, http://dx.doi.org/10.1002/cite.330340205.

[12] A. Cybulski, J.A. Moulijn, Monoliths in heterogeneous catalysis, Catal. Rev. 36 (2) (1994) 179–270, http://dx.doi.org/10.1080/01614949408013925.

[13] W. Tang, H. Zhou, Y. Zeng, M. Yan, C. Jiang, P. Yang, Q. Li, Z. Li, J. Fu, Y. Huang, Y. Zhao, Analysis on the convective heat transfer process and performance evaluation of triply periodic minimal surface (TPMS) based on diamond, gyroid and Iwp, Int. J. Heat Mass Transfer 201 (2023) 123642, http://dx.doi.org/10.1016/j.ijheatmasstransfer.2022.123642.

[14] I. Gräf, A.-K. Rühl, B. Kraushaar-Czarnetzki, Experimental study of heat transport in catalytic sponge packings by monitoring spatial temperature profiles in a cooled-wall reactor, Chem. Eng. J. 244 (2014) 234–242, http://dx.doi.org/10.1016/j.cej.2014.01.060.

[15] C. Sinn, J. Wentrup, G.R. Pesch, J. Thöming, Heat transport in open-cell foams: CFD analysis of artificial heat sources vs fully resolved exothermal reactions, Ind. Eng. Chem. Res. 60 (12) (2021) 4542–4551, http://dx.doi.org/10.1021/acs.iecr.0c05982.

[16] L. Biffar, W. Benzinger, P. Pfeifer, A simplified approach for calculating heat transfer coefficients for fluid guiding elements with alternating redirections of flow, Chem. Ing. Tech. 96 (8) (2024) 1116–1122, http://dx.doi.org/10.1002/cite.202300104.

[17] V. Meille, Review on methods to deposit catalysts on structured surfaces, Appl. Catal. A Gen. 315 (2006) 1–17, http://dx.doi.org/10.1016/j.apcata.2006.08.031.

[18] E. Santanach Carreras, F. Chabert, D.E. Dunstan, G.V. Franks, Avoiding mud cracks during drying of thin films from aqueous colloidal suspensions, J. Colloid Interface Sci. 313 (1) (2007) 160–168, http://dx.doi.org/10.1016/j.jcis.2007.03.076.

[19] L. Besra, M. Liu, A review on fundamentals and applications of Electrophoretic Deposition (EPD), Prog. Mater. Sci. 52 (1) (2007) 1–61, http://dx.doi.org/10.1016/j.pmatsci.2006.07.001.

[20] S. Shariffudin, S.H. Herman, M. Rusop, Layer-by-layer nanoparticles ZnO thin films prepared by sol-gel method, Adv. Mater. Res. 403–408 (2012) 1178–1182, http://dx.doi.org/10.4028/www.scientific.net/AMR.403-408.1178.

[21] C. Mochales, S. Frank, R. Zehbe, T. Traykova, C. Fleckenstein, A. Maerten, C. Fleck, W.-D. Mueller, Tetragonal and cubic zirconia multilayered ceramic constructs created by EPD, J. Phys. Chem. B 117 (6) (2013) 1694–1701, http://dx.doi.org/10.1021/jp3064432.

[22] B. Ferrari, S. González, R. Moreno, C. Baudín, Multilayer coatings with improved reliability produced by aqueous electrophoretic deposition, J. Eur. Ceram. Soc. 26 (1) (2006) 27–36, http://dx.doi.org/10.1016/j.jeurceramsoc.2004.10.018.

[23] D. Napper, Steric stabilization, J. Colloid Interface Sci. 58 (2) (1977) 390–407, http://dx.doi.org/10.1016/0021-9797(77)90150-3.

[24] B. Ferrari, R. Moreno, J.A. Cuesta, A resistivity model for electrophoretic deposition, Key Eng. Mater. 314 (2006) 175–180, http://dx.doi.org/10.4028/www.scientific.net/KEM.314.175.

[25] J. Gmehling, M. Kleiber, B. Kolbe, J. Rarey, Chemical Thermodynamics for Process Simulation, Second, completely revised and enlarged edition, Wiley-VCH, Weinheim, 2019.

[26] K. Aika, Preparation and characterization of chlorine-free ruthenium catalysts and the promoter effect in ammonia synthesis 3. A magnesia-supported ruthenium catalyst, J. Catal. 136 (1) (1992) 126–140, http://dx.doi.org/10.1016/0021-9517(92)90112-U.

[27] P. Sarkar, P.S. Nicholson, Electrophoretic deposition (EPD): Mechanisms, kinetics, and application to ceramics, J. Am. Ceram. Soc. 79 (8) (1996) 1987–2002, http://dx.doi.org/10.1111/j.1151-2916.1996.tb08929.x.

[28] F. Rosowski, A. Hornung, O. Hinrichsen, D. Herein, M. Muhler, G. Ertl, Ruthenium catalysts for ammonia synthesis at high pressures: Preparation, characterization, and power-law kinetics, Appl. Catal. A Gen. 151 (2) (1997) 443–460, http://dx.doi.org/10.1016/S0926-860X(96)00304-3.

[29] R. Javaid, T. Nanba, Stability of Cs/Ru/MgO catalyst for ammonia synthesis as a hydrogen and energy carrier, Energies 15 (10) (2022) 3506, http://dx.doi.org/10.3390/en15103506.

[30] Y.V. Larichev, B.L. Moroz, V.I. Zaikovskii, S.M. Yunusov, E.S. Kalyuzhnaya, V.B. Shur, V.I. Bukhtiyarov, XPS and TEM studies on the role of the support and alkali promoter in Ru/MgO and Ru-Cs + /MgO catalysts for ammonia synthesis, J. Phys. Chem. C 111 (26) (2007) 9427–9436, http://dx.doi.org/10.1021/jp066970b.

[31] H. Bielawa, O. Hinrichsen, A. Birkner, M. Muhler, The ammonia-synthesis catalyst of the next generation: Barium-promoted oxide-supported ruthenium, Angew. Chem. Int. Ed. 40 (6) (2001) 1061–1063, http://dx.doi.org/10.1002/1521-3773(20010316)40:6<1061::AID-ANIE10610>3.0.CO;2-B.

[32] C.J. Jacobsen, S. Dahl, P.L. Hansen, E. Törnqvist, L. Jensen, H. Topsøe, D.V. Prip, P.B. Møenshaug, I. Chorkendorff, Structure sensitivity of supported ruthenium catalysts for ammonia synthesis, J. Mol. Catal. A Chemical 163 (1–2) (2000) 19–26, http://dx.doi.org/10.1016/S1381-1169(00)00396-4.

[33] L. Li, Y.-F. Jiang, T. Zhang, H. Cai, Y. Zhou, B. Lin, X. Lin, Y. Zheng, L. Zheng, X. Wang, C.-Q. Xu, C.-t. Au, L. Jiang, J. Li, Size sensitivity of supported Ru catalysts for ammonia synthesis: from nanoparticles to subnanometric clusters and atomic clusters, Chem 8 (3) (2022) 749–768, http://dx.doi.org/10.1016/j.chempr.2021.11.008.

[34] A. Hellman, E.J. Baerends, M. Biczysko, T. Bligaard, C.H. Christensen, D.C. Clary, S. Dahl, R. van Harrevelt, K. Honkala, H. Jonsson, G.J. Kroes, M. Luppi, U. Manthe, J.K. Nørskov, R.A. Olsen, J. Rossmeisl, E. Skúlason, C.S. Tautermann, A.J.C. Varandas, J.K. Vincent, Predicting catalysis: Understanding ammonia synthesis from first-principles calculations, J. Phys. Chem. B 110 (36) (2006) 17719–17735, http://dx.doi.org/10.1021/jp056982h.

[35] H. Liu, Ammonia Synthesis Catalysts: Innovation and Practice, World Scientific Publishing, Singapore; Beijing, China, 2013, http://dx.doi.org/10.1142/8199,

[36] M. Thommes, K. Kaneko, A.V. Neimark, J.P. Olivier, F. Rodriguez-Reinoso, J. Rouquerol, K.S. Sing, Physisorption of gases, with special reference to the evaluation of surface area and pore size distribution (IUPAC Technical Report), Pure Appl. Chem. 87 (9–10) (2015) 1051–1069, http://dx.doi.org/10.1515/pac-2014-1117.